

## Article

# First-Principles and Experimental Study of Ge, V, Ta-Doped AgNi Electrical Contact Materials

Jingqin Wang<sup>1,2,\*</sup>, Yixuan Zhang<sup>2</sup>, Menghan Wang<sup>2</sup>, Jing Chen<sup>3</sup> and Guanglin Huang<sup>3</sup>

<sup>1</sup> Provincial and Ministerial Co-Construction Collaborative Innovation Center on Reliability Technology of Electrical Products, Tianjin 300130, China

<sup>2</sup> State Key Laboratory of Reliability and Intelligence of Electrical Equipment, Hebei University of Technology, Tianjin 300130, China; yxzhang818@163.com (Y.Z.); m15831390293@163.com (M.W.)

<sup>3</sup> Wenzhou Juxing Electric Contact Technology Co., Ltd., Wenzhou 325062, China; jxcj@china-juxing.cn (J.C.); jxhgl@china-juxing.cn (G.H.)

\* Correspondence: jqwang@hebut.edu.cn; Tel.: +86-022-60204354

**Abstract:** To explore the stability, electrical, and mechanical characteristics of undoped AgNi alongside AgNi doped with elemental Ge, V, and Ta, we performed calculations on their electronic structures using density functional theory from first-principles. We also prepared AgNi(17) and AgNi-x(Ge, V, Ta) electrical contact materials using the powder metallurgy technique, and they were subsequently assessed experimentally. The electrical properties of these materials were evaluated under a 24 V/15 A DC-resistive load using the JF04D contact material testing system. A three-dimensional morphology scanner was employed to examine the contact surface and investigate the erosion patterns of the materials. Our findings indicate that doping with metal elements significantly enhanced the mechanical properties of electrical contacts, including conductivity and hardness, and optimizes arc parameters while improving resistance to arc erosion. Notably, AgNi-Ge demonstrated superior conductivity and arc erosion resistance, showing significant improvements over the undoped AgNi contacts. This research provides a theoretical foundation for selecting doping elements aimed at enhancing the performance of AgNi electrical contact materials.

**Keywords:** AgNi electrical contact materials; first-principles calculations; electrical contact properties; morphological analysis



**Citation:** Wang, J.; Zhang, Y.; Wang, M.; Chen, J.; Huang, G. First-Principles and Experimental Study of Ge, V, Ta-Doped AgNi Electrical Contact Materials. *Coatings* **2024**, *14*, 629. <https://doi.org/10.3390/coatings14050629>

Academic Editor: Emilio Bellingeri

Received: 26 April 2024

Revised: 8 May 2024

Accepted: 15 May 2024

Published: 16 May 2024



**Copyright:** © 2024 by the authors. Licensee MDPI, Basel, Switzerland. This article is an open access article distributed under the terms and conditions of the Creative Commons Attribution (CC BY) license (<https://creativecommons.org/licenses/by/4.0/>).

## 1. Introduction

Contacts are essential components in switching appliances, and their performance directly affects the reliable operation and service life of switching appliances. In the selection of low-voltage electrical contact materials, it is necessary to consider a variety of characteristics including physical properties, mechanical properties, electrical contact properties, thermal properties, chemical properties, processing and manufacturing properties, and so on [1,2]. Ag-based electrical contacts are employed in a multitude of light- and heavy-load electrical appliances due to their resistance to electrical abrasion, resistance to fusion welding, high electrical conductivity with very low contact resistance, and chemical stability [3–5]. Ag-metal oxide is the most widely used electrical contact material; however, there are production problems due to the fact that the AgCdO material produces poisonous Cd vapors, and the AgSnO<sub>2</sub> has defects such as high hardness and an inability to withstand the stresses placed upon it by the wires [6–8]. AgNi contact material is a promising environmentally friendly alternative to traditional electrical contacts. It exhibits excellent electrical and thermal conductivity, low and stable contact resistance, a simple production process, and low cost. However, its resistance to fusion welding and abrasion under high-current conditions is poor, necessitating improvement of its various properties [9–12].

The majority of research on AgNi electrical contact materials has focused on improving the preparation process; however, relatively few studies have been conducted to improve

the properties of AgNi contact materials through additive doping. The physicochemical properties of additives can improve the electrical conductivity, wear resistance, and arc erosion resistance of electrical contact materials. This can significantly improve the mechanical properties and organization of AgNi alloys [13–15]. Some scholars have investigated that elemental doping can improve the electrical conductivity, arc erosion resistance, and other properties of AgNi electrical contact materials. For example, Wang et al. doped AgNi electrical contact materials with Re, In, and Nb elements, which led to an improvement in the micro-morphology of the contact surfaces and arc performance of the AgNi contact materials [16]. Lin et al. demonstrated that the addition of rare-earth elements to the contact materials could result in the formation of rare-earth oxides, which could be suspended in the molten silver pool at high temperatures [17]. This process was found to increase the viscosity, reduce material transfer, and improve the electrical properties of the contact materials. Wang et al. demonstrated that the addition of moderate quantities of CuO and Bi<sub>2</sub>O<sub>3</sub> to silver-based contact materials resulted in enhanced particle size and improved physical and electrical contact properties [18].

In this study, three elements, Ge, V, and Ta, were selected for the doping modification of the AgNi electrical contact materials. The physical properties, electrical properties, and arc erosion properties of the doped AgNi electrical contacts were investigated using a combination of first-principles calculations and specific experimental analyses. Firstly, the electronic structure and energy of the dopant-containing AgNi interface were calculated using the first-principles approach based on the density functional theory. Subsequently, the doped AgNi contact samples were prepared experimentally in order to obtain the hardness, conductivity, wettability, and other properties of the materials. X-ray diffraction experiments were conducted in order to verify the match between the prepared samples and the simulation model. Finally, the contact materials were analyzed for various electrical contact properties following electrical contact experiments. Following the completion of the electrical contact experiments, the electrical properties of the contact materials were analyzed. Additionally, the surface morphology of the electrical contacts was scanned and analyzed using a three-dimensional morphology scanner. The results demonstrated that Ge, V, and Ta doping had a positive impact on the properties of the AgNi electrical contact materials, with Ge-doped AgNi electrical contact materials exhibiting the most favorable performance. This outcome validated the consistency of the experimental results and the theoretical calculations derived from the simulation. This provides a novel concept and a more efficacious approach to enhancing the functionality of AgNi electrical contact materials.

## 2. Models and Calculation Method

Firstly, the geometry of the Ag and Ni cells was optimized in order to obtain stable structures with the lowest total energy. Based on the existing studies, among the binding forms at the AgNi interface, Ag(110)/Ni(211) has the highest interfacial binding energy [19]. In light of the interfacial mismatch inherent to the interfacial model, this study presented the establishment of an AgNi interfacial model with a 17% Ni content, based on Ag(110)/Ni(211) crystal surfaces. This model employed a superlattice model on the Ag(110) surface and a superlattice model on the Ni(211) surface, with each model comprising 4.5 and 2.5 layers, respectively. The surface of the Ag(110) was found to have 4.5 layers, while the Ni(211) surface exhibited 2.5 layers. The AgNi interfacial model with dopants is depicted in Figure 1, which also includes a 15 Å vacuum layer.

In this study, the calculations were performed with the CASTEP module of the Materials Studio software (<https://www.3ds.com/>), which was based on the first-principles approach of density functional theory, the calculations were performed in the inverse easy space, and the simulations were widely used in the calculation of ceramics, semiconductors, and metals that had periodic structure materials [20]. The ultrasoft pseudopotential was chosen to describe the interactions between valence electrons and ions for the performance simulation calculations of the AgNi(17) interface model, and the exchange-correlation

energies were treated using the PBE generalization under the generalized gradient approximation [21]. The BFGS algorithm was used to simulate the Ge, V, and Ta-doped AgNi interfacial model, taking the plane wave truncation energy as 517 eV, with the K-points in the Brillouin source region set to  $2 \times 9 \times 1$ , the total energy of SCF self-consistently convergence less than  $1.0 \times 10^{-5}$  eV/atom, the average atomic stress less than 0.5 eV/nm, the tolerance shift less than 0.02 nm, and the maximum stress deviation as 0.1 GPa. The valence electron configurations considered in the calculations are Ag:  $4d^{10}5s^1$ , Ni:  $3d^84s^2$ , Ge:  $4s^24p^2$ , V:  $3d^34s^2$ , and Ta:  $5d^36s^2$ .

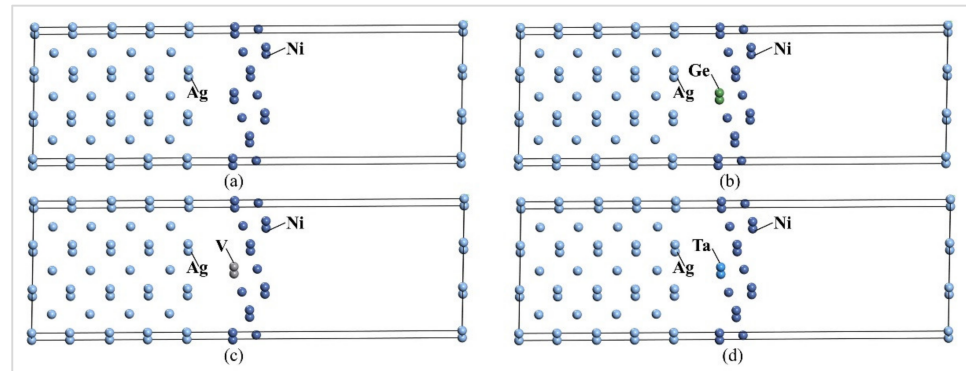


**Figure 1.** Interface model: (a) AgNi(17), (b) Ge-doped AgNi, (c) V-doped AgNi, and (d) Ta-doped AgNi.

### 3. Simulation Analysis

After geometry optimization for the doped AgNi interfacial model, energy calculations were performed on the interfacial model to analyze the interfacial bond strength, interfacial stability, and electronic structure.

#### 3.1. Interface Bond Strength

Two parameters, interfacial work of separation and interfacial energy, are introduced to analyze the stability and interfacial bond strength of Ge-, V-, and Ta-doped AgNi interfacial bonding [22].

The work of interfacial separation ( $W_{sep}$ ) is the energy required to separate a unit area of an interface into separate interfaces, calculated by the formula:

$$W_{sep} = \frac{E_{Ag}^{slab} + E_{Ni}^{slab} - E_{AgNi}^{inter}(relax)}{A} \quad (1)$$

where  $E_{Ag}^{slab}$  and  $E_{Ni}^{slab}$  are the total energies of the Ag/Ni free surface model, respectively;  $E_{AgNi}^{inter}(relax)$  is the total energy of the relaxed AgNi interface model; and  $A$  is the area of the interface model.

The interfacial energy ( $\gamma_{int}$ ) is the value of the energy change of an interface within a unit area due to atomic distortion, changes in metallic bonding, and structural strain, calculated as:

$$\gamma_{int} = \sigma_{Ag} + \sigma_{Ni} - W_{sep} \quad (2)$$

where  $\sigma_{Ag}$  and  $\sigma_{Ni}$  are the surface energies of Ag and Ni free surfaces, and  $W_{sep}$  is the separation work at the AgNi interface.

Table 1 shows the calculation results of interfacial separating work and interfacial energy for Ge-, V-, and Ta-doped AgNi. From the data in the table, it can be found that the interfacial separation work and interfacial energy of AgNi(17) and Ge-, V-, and Ta-doped AgNi interfacial models are all positive values, indicating that these interfacial models can be stabilized.

**Table 1.** Separation work and interfacial energy.

Model	$W_{\text{sep}}$ (eV/Å <sup>2</sup> )	$\sigma_{\text{Ag}}$ (eV/Å <sup>2</sup> )	$\sigma_{\text{Ni}}$ (eV/Å <sup>2</sup> )	$\gamma_{\text{int}}$ (eV/Å <sup>2</sup> )
AgNi(17)	0.0210	0.0436	0.1476	0.1702
AgNi-Ge	0.0491	0.0436	0.1355	0.1300
AgNi-V	0.0361	0.0436	0.1428	0.1503
AgNi-Ta	0.0329	0.0436	0.1533	0.1640

The interfacial work of separation  $\sigma$  and interfacial energy of the undoped AgNi(17) interface model are 0.0210 eV/Å<sup>2</sup> and 0.1702 eV/Å<sup>2</sup>, respectively, and the interfacial work of separation of the Ge-, V-, and Ta-doped interface are increased compared with that of the pre-doped interface, which indicates that the interfacial atoms are more capable of bonding to each other and that the interfacial bonding is stronger, of which the Ge-doped interface has the highest interfacial bonding strength. The interfacial energy of the AgNi interface decreases after doping, indicating that the incorporation of Ge, V, and Ta atoms increases the stability of the interface, among which the Ge-doped interface is the most stable. Since the radius and electronegativity of the dopant atoms are different from those of the Ni atoms, the introduction of dopant atoms may make the lattice constants of the AgNi interface distorted, thus affecting the stability of the interface.

### 3.2. Density of States Analysis

The density of states can be used to reflect the interaction between dopant atoms and other atoms, as well as the formation of chemical bonds in crystals, and is an important parameter for analyzing the electronic structure of materials [23]. The density of states image is shown in Figure 2, where the total density of states (TDOS) indicates the state of the energy distribution of all the electrons in the system, and the fractional-wave density of states indicates the bonding of electrons in different orbitals.

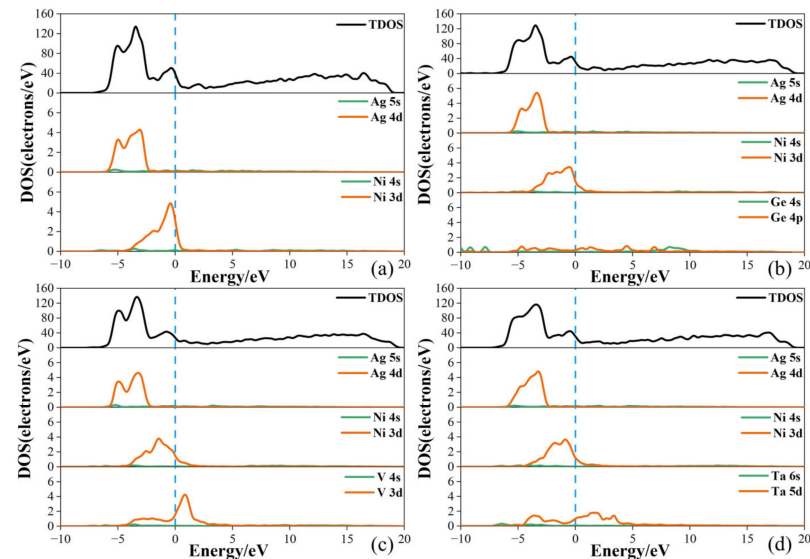


**Figure 2.** Density of states. (a) AgNi(17), (b) Ge-doped AgNi, (c) V-doped AgNi, and (d) Ta-doped AgNi.

Figure 2a shows the density of states image of undoped AgNi(17), in which it can be seen that the number of electrons near the Fermi energy level (energy of 0 eV) is higher, which indicates that AgNi(17) has good electrical conductivity. The energies of AgNi(17) are concentrated in the range of  $-10\sim 20$  eV, which are mainly contributed by the 5 s, 4 d orbitals of the Ag element and the 4 s, 3 d orbitals of the Ni element. At  $-7\sim 0$  eV, the wave peaks of AgNi mainly originate from the d orbitals of Ag elements, and the d orbitals of Ni elements contribute, and at  $-4\sim -2$  eV, there are obvious overlapping peaks of Ag-d

orbitals and Ni-d orbitals. This hybridization can reflect the formation of metal bonds, and the strength of hybridization is positively correlated with the stability of bonding.

From the density of states images of Ge-doped AgNi in Figure 2b, it can be seen that the density of states of Ag atoms in the valence band region shifts to the low-energy region as a whole, and the density of states of Ni atoms shifts to the Fermi energy level as a whole, compared with the density of states of undoped AgNi, and the density of states images of Ag atoms in the valence band region shows two peaks in the range of  $-8\sim-0$  eV, which is mainly contributed by the participation of the Ag-d orbitals, the Ni-d orbitals, and the Ge-p orbitals. In the range of  $-4\sim-0$  eV, Ag-d orbitals, Ni-d orbitals, and Ge-p orbitals are hybridized, which implies enhanced interatomic interactions and stronger metal bonding. The fractional density of states waveform curves of Ge are relatively flat, with no localized spikes in the s- and p-band orbitals, and the nonlocalized nature of the Ge electrons is strong, and compared with the un-doped AgNi system, the number of carriers of the Ge-doped system and the electrical properties are enhanced.

Figure 2c shows the density of states images of V-doped AgNi; compared with the density of states images of undoped AgNi, the density of states of Ag atoms in the valence band region moves to the low energy region as a whole, and the density of states of Ni atoms moves to the Fermi energy level as a whole. The density of states peaks in the  $-8\sim-3$  eV region of the density of states images are mainly contributed to by the hybridization of the Ag-d orbitals, the Ni-d orbitals, and the V-d orbitals. V doping increases the hybridization levels of the Ag-d orbitals and the Ni-d orbitals. The hybridization level of Ag-d and Ni-d orbitals, the strong metal bonding ability between Ni and V, the existence of a large energy spike in the 3d orbital of V, the strong electronic localization of its orbitals, the narrower energy bands, and the doping of V increases the conductivity of AgNi.

Figure 2d shows the density of states image of Ta-doped, which is similar to that of Ge- and V-doped AgNi, with the density of states of Ag atoms in the valence band region moving to the low energy region as a whole, and the density of states of Ni atoms moving to the Fermi energy level as a whole. The dopant atom Ta has an effect in both the valence band and conduction band energy regions. Ag-d orbitals, Ni-d orbitals, and Ta-d orbitals are hybridized in the range of  $-10\sim-1$  eV, and they produce interactions as bonding orbitals. In the region of  $1\sim5$  eV, the main contribution comes from Ta-d orbitals.

By analyzing the density of states, it can be concluded that the doping of Ge, V, and Ta can improve the electrical conductivity of AgNi contact materials, which provides a theoretical basis for the study of doping to improve the electrical properties of contact materials.

### 3.3. Mulliken Population Analysis

Electronic structure characteristics determine the interfacial bonding strength and interfacial stability and will ultimately affect the material properties. The distribution of electrons in atomic orbitals can be determined by integrating the number of electrons from the density of states diagram, but it is difficult to quantitatively characterize the strength of bonding, and it is necessary to carry out the Mulliken population analysis to determine that the strength of bonding is based on the value of the layout [24].

The charge population is used to characterize the transfer of electrons between atoms. A positive charge population indicates that atoms are prone to lose electrons; on the contrary, a negative charge population indicates that atoms are more likely to gain electrons. The larger the absolute value of the population, the stronger the ability of the atom to gain or lose electrons. Table 2 shows the average charge population obtained by simulation, before and after doping, and the ability of each atom to gain and lose electrons changes. The charge population of Ag atoms is negative and the charge population of Ni atoms is positive, indicating that Ag loses electrons in electron transfer and Ni gains electrons in electron transfer in the interface of AgNi. Also, Ge doping strengthens the electron-losing ability of Ag and the electron-gaining ability of Ni, strengthens the interaction between the atoms, and makes the electron transfer at the AgNi interface more obvious, which is conducive to enhancing the stability of the interfacial bonding, whereas V and Ta doping

weakens the electron-gaining and electron-losing abilities of Ag and Ni atoms, respectively.

**Table 2.** Atom population.

Model	Atom Population(e)				
	Ag	Ni	Ge	V	Ta
AgNi(17)	−0.0041	0.0141			
AgNi-Ge	−0.0058	0.0172	0.2210		
AgNi-V	−0.0034	0.0091		0.1330	
AgNi-Ta	−0.0027	0.0135			0.1700

The bond population is used to characterize the nature of interatomic bonding. The larger the absolute value of the bond population, the more the electron clouds overlap with each other, the stronger the interatomic bonding ability, and the more stable the chemical bond formed. Table 3 shows the average values of the bond population obtained by simulation. The increase of bond population between Ag-Ni after Ge, V, and Ta doping indicates that the metal bonding between Ag-Ni is enhanced, the orbital charge is increased in different degrees, and the interaction between Ag and Ni atoms is enhanced, which improves the bonding stability at the AgNi interface. Also, the bond overlap population between Ni-Ni is increased after Ge and Ta doping. The increase of Ni-Ge, Ni-V, and Ni-Ta bonding at the doped interface also enhances the bonding strength of the AgNi interface.

**Table 3.** Bond population.

Material	Bond Population(e)		
	Ag-Ni	Ni-Ni	Ni-X
AgNi(17)	0.27	0.17	
AgNi-Ge	0.43	0.31	0.15
AgNi-V	0.33	0.15	0.05
AgNi-Ta	0.37	0.21	0.07

## 4. Experiment

### 4.1. Preparation of Doped-AgNi Contact Materials by Powder Metallurgy

In this study, AgNi and Ge-, V-, and Ta-doped AgNi electrical contact materials were prepared by the powder metallurgy method. Firstly, the weighed powders were powder mixed using a high-energy ball mill, so that the doped Ge, V, Ta powders and Ag, Ni powders were fully mixed in the ball mill, and after powder drying, they were subjected to primary pressing, primary firing, re-pressing, re-firing, and secondary re-pressing, and then they were ground, polished, and wire-cut to obtain the finished product of electrical contacts with a diameter of 3.2 mm and a height of 2.5 mm. The flow chart for the preparation of electrical contact samples is shown in Figure 3.

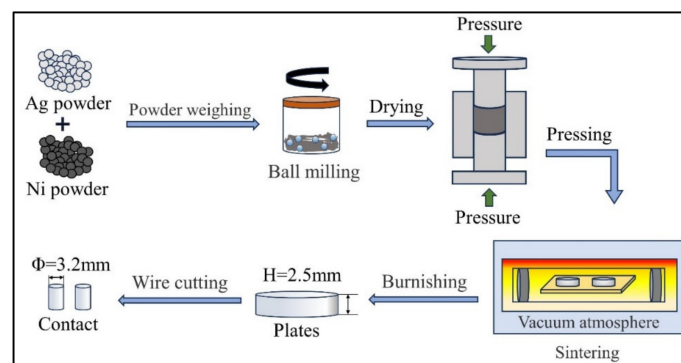


**Figure 3.** Process flow diagram for the preparation of doped AgNi electrical contact materials.

The samples of AgNi and AgNi contacts containing Ge, V, and Ta doping were prepared in this experiment as 10 g. The atomic ratios and mass of each component are shown in Table 4, and the purity of chemicals is shown in Table 5.

**Table 4.** Main raw material ratios.

Material	Atomic Ratio	Mass Ratio
AgNi(17)	73:27	83.23%:16.77%
AgNi-Ge	73:24.3:2.7	82.92%:15.02%:2.06%
AgNi-V	73:24.3:2.7	83.43%:15.11%:1.46%
AgNi-Ta	73:24.3:2.7	80.44%:14.57%:4.99%

**Table 5.** Purity of chemicals.

Name of Chemicals	Purity
Ag powder	≥99.9%
Ni powder	≥99.5%
Ge powder	≥99.9%
V powder	≥99.9%
Ta powder	≥99.9%
Anhydrous ethanol C <sub>2</sub> H <sub>5</sub> OH	≥99.9%

#### 4.2. X-ray Diffraction Experiment (XRD)

In order to confirm the match between the doped AgNi materials prepared by powder metallurgy and the replacement doping model established by simulation, this study utilized a SmartLab X-ray diffractometer to analyze the physical phase of the AgNi contact materials before and after doping. The diffractometer adopted Cu-targeted K $\alpha$ -ray scanning, with a power of 3 kW, wavelength of 0.15405 nm, and a scanning angle range of 10°~90°. The scanning speed was 6°/min. The X-ray diffraction results are shown in Figure 4, the diffraction peaks of AgNi contact materials before and after doping are basically in the same angular position, and the XRD peaks are slightly deviated, which may be caused by the introduction of dopants to make the AgNi interface undergo a slight aberration. However, there are no new peaks, which indicates that the doped AgNi contact materials do not generate a new phase, and the crystalline structure remains unchanged, implying that the powder metallurgy process has not changed. This means that the powder metallurgy process has successfully doped Ge, V, and Ta into the AgNi material and realized the replacement doping, which proves consistency between the prepared AgNi contact material and the simulation model.

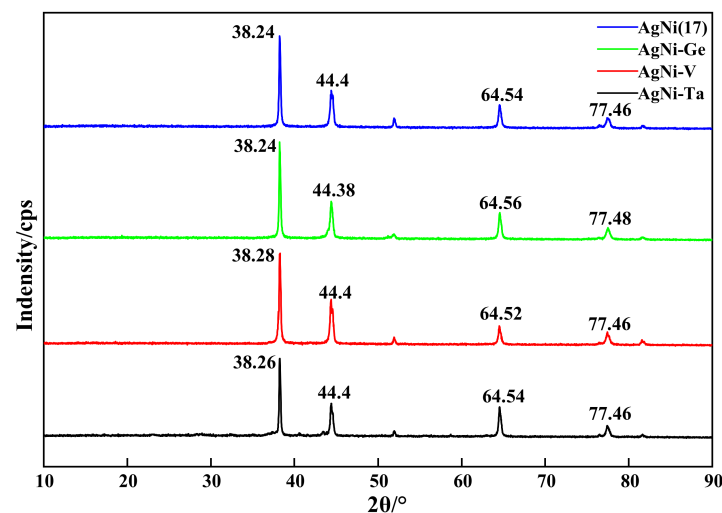


**Figure 4.** X-ray diffraction pattern.

The crystal size can be estimated using the Scherrer equation from the peak spreading of the XRD diffraction pattern (Full Width at Half Maximum (FWHM) of the peaks). The Scherrer equation is shown below:

$$D = \frac{K\lambda}{\beta \cos\theta} \quad (3)$$

where  $D$  is crystal size,  $K$  is the Scherrer constant,  $\lambda$  is the X-ray wavelength,  $\beta$  is the Peak width after instrumental effects, and  $\theta$  is the Bragg diffraction angle.

The calculated crystal size of AgNi before and after Ge, V, and Ta doping is shown in Table 6. The results show that the Ge, V, and Ta doping of AgNi forms a stable transition metal phase, which leads to an increase in lattice strain and promotes grain refinement, resulting in a smaller crystal size.

**Table 6.** Crystal size before and after doping.

Material	Crystal Size (nm)
AgNi(17)	38.66
AgNi-Ge	30.91
AgNi-V	35.86
AgNi-Ta	35.25

#### 4.3. Wettability Analysis

Wettability can evaluate interfacial bonding strength and the wettability experiment can verify the correctness of the simulation calculation results. In this study, the seated droplet method was chosen to test the wettability relationship between the two phases of intrinsic Ni or Ni containing dopants (Ge, V, Ta) as a solid substrate and Ag. Figure 5 shows the test results of the wettability angle. Figure 5a shows the spreading effect of Ag droplets in a molten state on the Ni substrate, and the wetting angles on both sides are  $87.2^\circ$  and  $83.6^\circ$ , which are close to  $90^\circ$ , respectively. From Figure 5b–d, it can be seen that the wetting angles of the doped AgNi were all reduced, with average values of  $27.6^\circ$ ,  $76.8^\circ$ , and  $77.5^\circ$ , respectively, which were smaller than the average value of  $85.4^\circ$  of the wetting angle of the undoped AgNi(17), wherein the Ge-doped AgNi contact material had the smallest wetting angle and the best wettability. The V- and Ta-doped AgNi material also improved the wettability of AgNi contact materials, confirming the correctness of the simulation calculation and analysis method of the first-principles approach based on density functional theory.

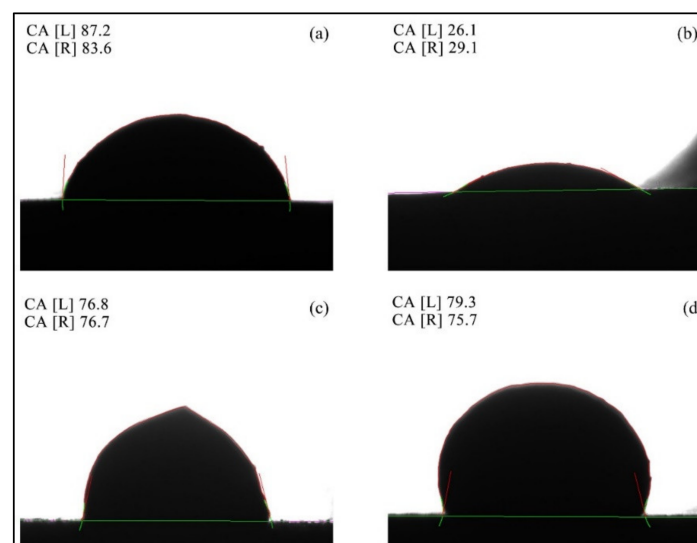


**Figure 5.** Wetting angle: (a) AgNi(17), (b) Ge-doped AgNi, (c) V-doped AgNi, and (d) Ta-doped AgNi.

In the actual use of the process, the wettability of the contact material in the arc can make more Ni particles dissolve in the Ag melting pool, causing the formation of a uniformly dispersed distribution of AgNi alloy to improve the AgNi interfacial bonding strength to prevent spattering loss due to arc erosion and help to improve the arc performance of the AgNi contact material.

#### 4.4. Electrical Contact Experiment

In this study, the JF04D electrical contact material test system was used to conduct electric contact arc erosion experiments, and the structure of the JF04D test system is shown in Figure 6. The test system can simulate the electric contact in the actual operation of the process, the moving contact is the anode contact, the static contact is the cathode contact, and the device can collect the arc energy, arc duration, welding force, contact resistance, and other experimental data. The experimental conditions of the electrical contact test experiment are detailed in Table 7.

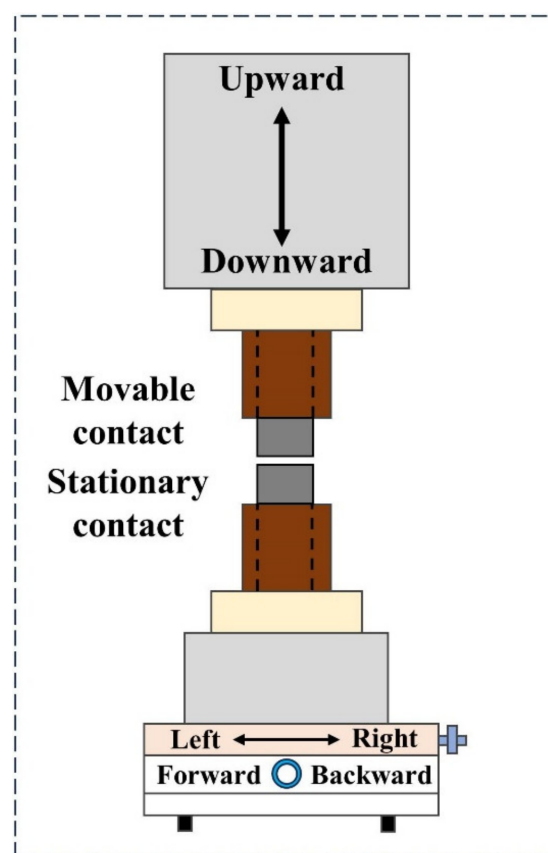


**Figure 6.** JF04D electrical contact test system.

**Table 7.** Electrical contact test conditions.

Parameter	Value
Power type	DC
Voltage/V	24
Current/A	15
Gas environment	Air
Closing pressure/cN	86
Operation times	100,000
Load type	Resistance

During the electrical contact process, cyclic arc discharge, contact stress, and Joule heat inevitably affect the surface condition of the electrical contact material, leading to

metal melting, sputtering, vaporization, and oxidation, which ultimately reduces the surface contact properties of the electrical contact material, leading to deterioration in performance [25–27]. Therefore, it is of great theoretical and practical significance to study the physical properties of electrical contact materials and to evaluate the degree of erosion of electrical contact materials in the arc erosion process.

#### 4.4.1. Arc Energy and Arc Duration Analysis

Arc energy and arc duration are important indicators of arc erosion resistance of electrical contact materials. In order to deeply study the arc stability of doped AgNi electrical contact materials with various elements, this study adopts the JF04D electrical contact material testing system and selects Ge-, V-, and Ta-doped AgNi contact materials as the anode of the asymmetric pair for the experimental study on electrical contacts. The measured data were divided into 100 data points (the average value of every 1000 operations was taken as one data point), the mean and standard deviation (S.D.) were calculated for each set of data, and the change curves of each parameter with the number of operations were plotted. Figure 7 shows the graph of the change of arc energy with the number of operations. It can be seen that the arc energy with the highest increase in the number of operations is an upward trend, in which the undoped AgNi contact material has the largest increase, the arc energy of the mean and standard deviation of the arc energy is the largest, the fluctuation is more obvious, and the doping of the average value of the arc energy and standard deviation of the AgNi contact material have been reduced to a certain degree, indicating that the doping to improve the AgNi contact material arc energy has a certain effect. In Figure 8, the opening arc duration with the number of operation curves can be seen. The arc time trend and arc energy trend is similar. Before and after the doping of the AgNi contact material, the arc duration of the average value and variance of the arc time have changed to some extent, the doped contact material arc duration of the average value of the arc time has been reduced, and at the same time, the standard deviation of the arc duration in the various elements of the doped contact material have been reduced, the change of fluctuations has decreased, and the change of the arc duration is more stable. In summary, the arc stability of the four contact materials is ranked as follows: AgNi-Ge > AgNi-Ta > AgNi-V > AgNi, which is consistent with the simulation results of thermal stability. Therefore, elemental doping is suitable for improving the arc erosion resistance and arc stability of AgNi contact materials, while Ge doping is most effective for reducing arc energy and improving arc stability.

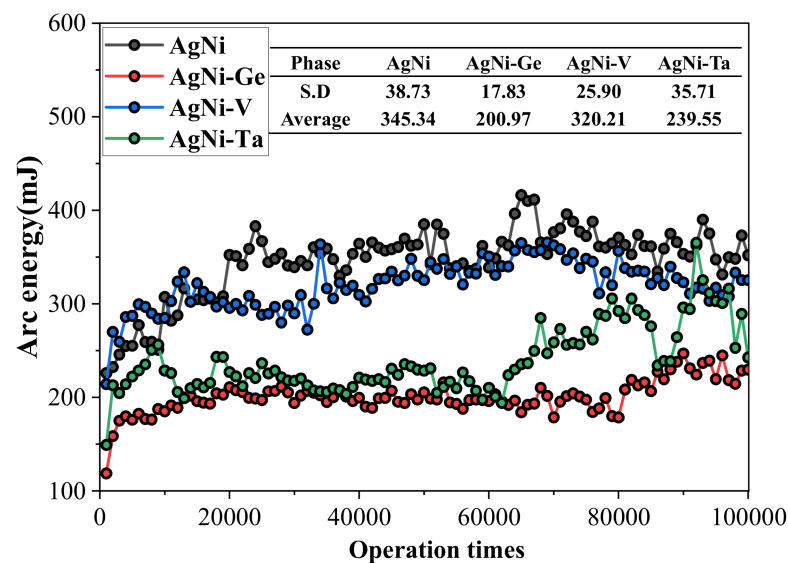


Figure 7. Plot of the variation of break arc energy with the number of operations.

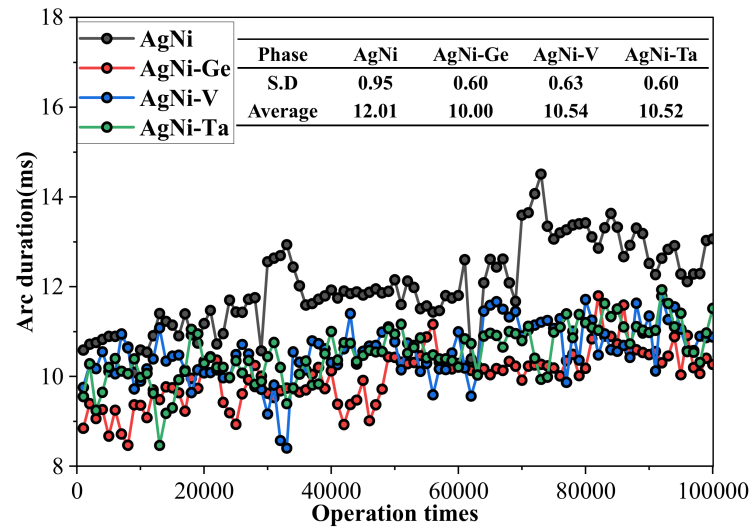


Figure 8. Plot of the variation of break arc time with the number of operations.

#### 4.4.2. Welding Force Analysis

The value and fluctuation of a welding force can reflect the welding resistance of a material, in which the current passes through the closed contacts, leading to the occurrence of contact melting and contact welding. The smaller the welding force of the electrical contact, the stronger the resistance of the contact material to welding. Figure 9 shows the curve of the welding force with the number of operations. At 50,000 and 70,000 operations, the welding force of the undoped AgNi contact material undergoes a large degree of mutation; the average value of its welding force is 84.57 cN, with a standard deviation of 7.97, and the average value of the welding force of the Ge- and Ta-doped AgNi contact material is 83.34 cN and 76.04 cN respectively. The standard deviation is 6.61 and 7.02, respectively, which are smaller than the mean value and standard deviation of undoped AgNi contacts, and the welding force curve is more gentle, indicating that the doping of Ge and Ta makes the AgNi contact material more stable and less prone to softening or melting and inhibits the movement of the material's grain boundaries, which strengthens the stability of the grain interfaces and the interfacial bonding strength of the AgNi contact material and improves the welding force of the contact material. The V doping may make the surface of the AgNi contact material not smooth or uniform enough, resulting in a slight decrease in the anti-melting performance. The experimental results show that doping can improve the anti-melting performance of AgNi contact materials to a certain extent.

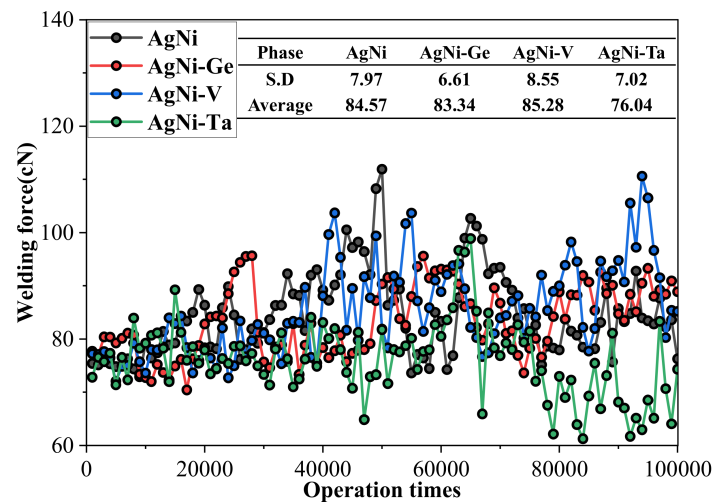


Figure 9. Plot of the variation of break welding force with the number of operations.

#### 4.4.3. Contact Resistance Analysis

Contact resistance usually occurs where two conductors are in contact with each other, and this resistance is caused by incomplete contact of the contact surfaces or non-smoothness of the contact surfaces [28]. The contact working process of the actual contact surface is not absolutely flat and there is a slight unevenness, so the essence of the contact is the raised peaks of the mutual contact. The current through the larger cross-section of the conductor to the tiny contact point occurs when the violent contraction, accompanied by this phenomenon, produces an additional resistance that is the contact resistance. In addition, due to the processing of the residue of the dust, abrasiveness, and other conductive substances, such as the pollution of the poorer conductive material or contact surface, a film resistance forms [29,30]. Doped AgNi contact material contact resistance with the number of operations changes in the curve are shown in Figure 10. As an overall view, the AgNi contact material contact resistance values first decrease and then increase (there is an increase in the number of operations and fluctuations in the reduction) and then tend to be relatively stable, indicating that the arc action of the surface morphology and composition of the contact changes each time after the closure of the contact occurs. After the raised peaks are remelted and solidified, the actual contact area and contact location between the contacts changes continuously, and the deposition and oxidation of Ni on the surface make the contact resistance increase and level off. The average and standard deviation of the contact resistance of the undoped AgNi contact materials are 5.15 mΩ and 0.75, respectively. After doping, the contact resistance of the contact materials is generally reduced, and the fluctuation amplitude is also reduced, which indicates that the introduction of doping elements improves the quality of the contact interface, which can improve the efficiency of the current transmission, thus reducing the contact resistance.

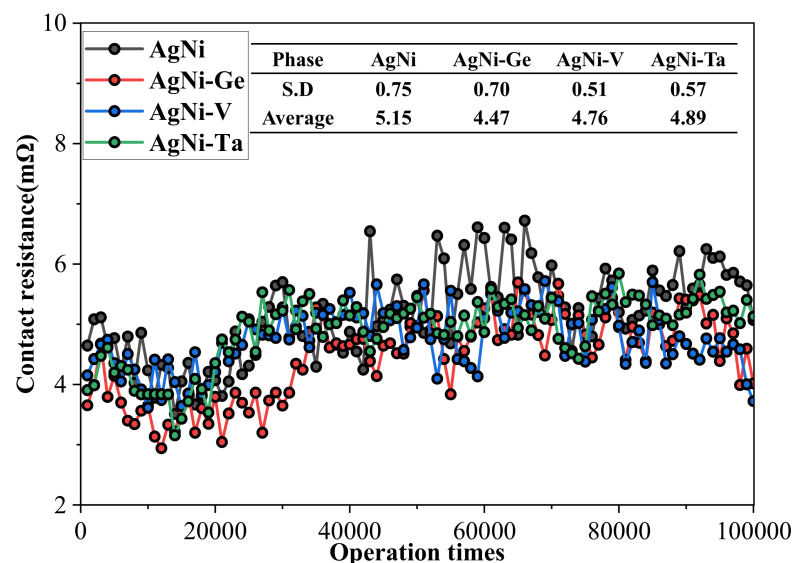
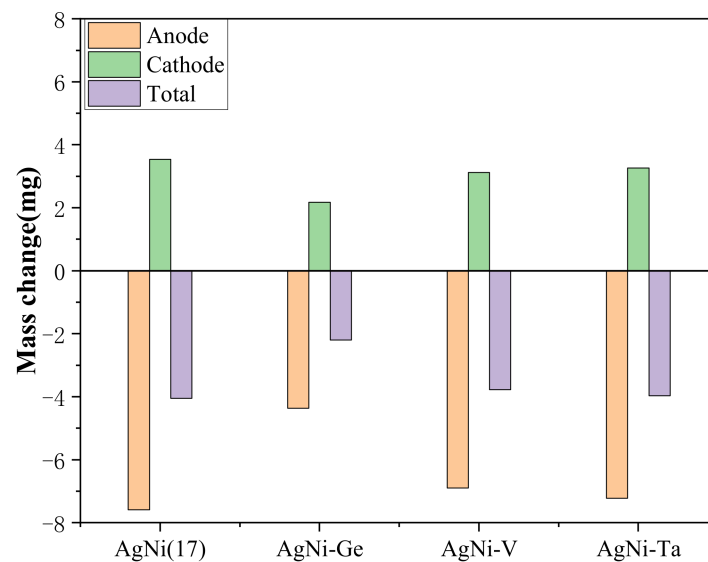


Figure 10. Plot of the variation of contact resistance with the number of operations.

#### 4.4.4. Material Transfer Analysis

When the arc discharges, the surface of the electrical contact evaporates and splashes, causing damage to the electrical contact and material loss. Material transfer and material loss are important indicators for evaluating the life of electrical contacts. After completing an electrical contact test experiment with 100,000 on-off operations, the mass change of the contacts was measured using a ME235S electronic balance of the Sartorius Genius series, and Figure 11 shows the mass change of the anode and cathode of the contact material, as well as the total mass loss due to arc erosion. Before doping, the material transfer and total mass loss of AgNi(17) electrical contacts were high, the total mass loss of AgNi contact materials after doping were decreased, and the material transfer from anode to cathode

contacts was also improved to some extent compared with that before doping, with a significant reduction in material transfer, in which the AgNi-Ge contact material showed the least material transfer and material loss, indicating that it has better electrical properties, arc erosion resistance, and high thermal stability, and the possibility of degradation under the influence of arc is smaller. The degree of mass loss of the contact material agrees well with the simulation results of the thermal stability analysis of the doped AgNi material, which confirms that the doping can improve the thermal stability performance of the AgNi contact material.



**Figure 11.** Mass change of the electrical contact material after 100,000 operations.

#### 4.4.5. Arc Erosion Morphology Analysis

By studying the arc erosion morphology of electrical contacts, the arc erosion resistance of AgNi doped contact materials can also be analyzed. In this study, an Olympus digital microscope DSX1000 was used to scan the three-dimensional morphology of the anode contact material after completing 100,000 operations, and the scanned results were imported into the Origin plotting software (<https://www.originlab.com/>) to draw the three-dimensional macroscopic morphology of the contact, as shown in Figure 12. It can be seen that the surface morphology of the undoped AgNi contacts changed significantly after arc erosion, producing large pits on the surface, and the surface morphology of the Ge-, V-, and Ta-doped anode contacts improved significantly after arc erosion, with no deeper pits and a flatter surface. The ablation area of the Ge-doped AgNi contact material was obviously reduced, the ablation depth was smaller, and the surface ablation morphology of the V- and Ta-doped AgNi contact material tended to be dispersed, which made the ablation of the contact surface more uniform. Therefore, it was initially concluded that the doping of Ge, V, and Ta improved the arc erosion resistance of the AgNi electrical contact material.

If the three-dimensional macroscopic morphology of the electrical contact after arc erosion is only observed, it cannot accurately represent the ablation of the electrical contact material, so it will be more intuitive and precise to extract the parametric features of the contact surface morphology to analyze the contact morphology. Therefore, this study introduces three surface roughness parameters,  $Sq$ ,  $Sz$ , and  $Sa$ , to reflect the erosion of the contact surface, and the following are the definitions and calculation formulas of the three roughness parameters [31–33]:

Root mean square height ( $Sq$ ): Represents the root mean square for  $Z(x, y)$  within the evaluation area. The parameter generates good statistics and enables stable results since

the parameter is not significantly influenced by scratches, contamination, and measurement noise:

$$Sq = \sqrt{\frac{1}{A} \iint_A Z^2(x,y) dx dy} \quad (4)$$

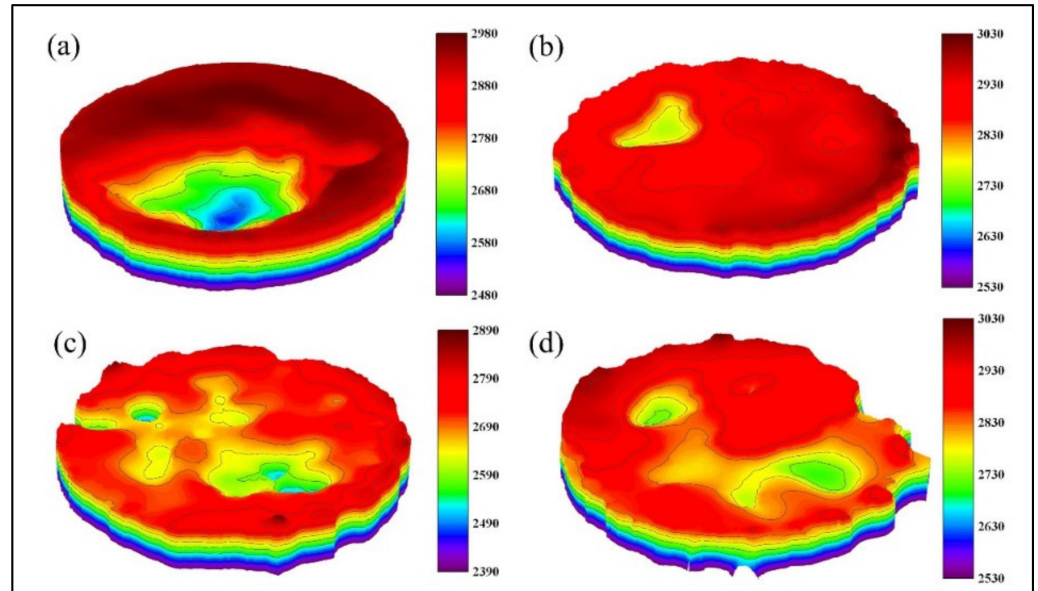


**Figure 12.** Contact three-dimensional morphology: (a) AgNi(17), (b) Ge-doped AgNi, (c) V-doped AgNi, and (d) Ta-doped AgNi.

Maximum height ( $Sz$ ): The maximum height  $Sz$  is equivalent to the sum of the maximum peak height  $Sp$  and maximum valley depth  $Sv$ :

$$Sz = \max(Z(x,y)) + |\min(Z(x,y))| \quad (5)$$

Arithmetical mean height ( $Sa$ ): Represents the arithmetic mean of the absolute ordinate  $Z(x,y)$  within the evaluation area and is the mean of the average height difference for the average plane:

$$Sa = \frac{1}{A} \iint_A |Z(x,y)| dx dy \quad (6)$$

The surface morphology information matrix of the contacts was obtained by scanning, and the surface roughness parameters corresponding to each contact material were calculated by the least-squares method to construct the reference plane so as to analyze the roughness degree of the contact surface and judge the arc erosion resistance of the doped AgNi contact material. The surface roughness parameters of the contact material are shown in Table 8.  $Sq$ ,  $Sz$ , and  $Sa$  are 457.669  $\mu\text{m}$ , 792.095  $\mu\text{m}$ , and 447.425  $\mu\text{m}$ , respectively, indicating that the protrusion height and pit depth on the surface of the contact are large and the three roughness parameters of the doped AgNi contact material are reduced, indicating that the surface ablation of the doped AgNi contact material is relatively flat, there are no huge protrusions and pits, and the ablation area is more homogeneous, which is consistent with the results of the 3D macroscopic morphological analysis, indicating that the doping of Ge, V, and Ta plays the role of grain refinement, so that the doped AgNi contact material presents a flatter overall shape. This further confirms that the doping of Ge, V, Ta can enhance the arc erosion morphology of AgNi contact material and improve the arc erosion resistance of the contact material, which provides an effective idea and analytical method for the study of doping to improve the arc erosion resistance of contact materials.

**Table 8.** Surface roughness.

Material	Sq ( $\mu\text{m}$ )	Sz ( $\mu\text{m}$ )	Sa ( $\mu\text{m}$ )
AgNi(17)	457.669	792.095	447.425
AgNi-Ge	400.541	678.712	396.836
AgNi-V	391.546	781.540	385.411
AgNi-Ta	298.472	773.896	292.514

#### 4.5. Other Physical Property Analysis

The hardness and conductivity were experimentally determined, as shown in Table 9. Compared with the undoped AgNi contact material, the hardness and conductivity of the Ge-, V-, and Ta-doped contact materials have been changed to a certain extent, in which the conductivity and hardness of the Ge-doped AgNi contact material have been greatly improved, which indicates that the doping of Ge makes the crystal structure of the material aberrated so that the crystal structure is more compact and stable, improving the hardness of the contact material. At the same time, the doping of Ge changes the electronic structure of the material so that the free electron movement in the crystal structure becomes more efficient, reducing the scattering of electrons and improving the electrical conductivity of the AgNi contact material. V- and Ta-doped AgNi contact material conductivity has been improved to a certain extent and the hardness is slightly decreased, which indicates that after the doping of the dislocations are introduced or the crystal structure is changed so that the material is easier to occur in the plastic deformation, the toughness has been improved. The experimental results confirm the theoretical analysis.

**Table 9.** Hardness and conductivity.

Material	Hardness (HV)	Conductivity (IACS%)
AgNi(17)	88.149	37.0
AgNi-Ge	98.602	44.3
AgNi-V	86.960	38.2
AgNi-Ta	86.995	38.2

## 5. Conclusions

In this study, the interfacial stability and electronic structure of undoped AgNi as well as Ge-, V-, and Ta-doped AgNi were investigated using first-principles calculations. The arc performance and physical properties of the prepared AgNi doped electrical contact samples were also analyzed experimentally. The findings of this study indicate:

- (1) The simulation results show that the stability, electrical conductivity, and physical properties of the doped materials are improved to some extent. Specifically, the Ge-doped materials have the highest electrical conductivity, and their hardness is also improved. V- and Ta-doped materials have improved electrical conductivity, but their hardness is reduced; however, their toughness is enhanced;
- (2) It is demonstrated that the incorporation of Ge, V, and Ta elements has a significant effect on the arc behavior of AgNi electrical contact materials. Specifically, the doping enhances the electrical conductivity of the contact material, which is consistent with the simulation results, and at the same time reduces the contact resistance of the material, shortens the arc duration, reduces the arc energy, smooths the arc gradually, and reduces the welding force. Three-dimensional morphology analysis shows that the doping of Ge, V, and Ta elements reduces the cracks, holes, and bumps on the material surface and significantly reduces the arc erosion. Overall, the addition of Ge, V, and Ta elements improved the physical and electrical properties of the contact materials and enhanced their resistance to arc erosion;
- (3) The doping effect of Ge was the most significant. This doping resulted in the most significant increase in the electrical conductivity of the contact material; moreover,

the average arc duration and arc energy were minimized. In addition, the erosion of the material surface was more uniform, without obvious cracks and holes, and the material transfer and mass loss were relatively small. Therefore, the Ge element has the best enhancement effect on the resistance of AgNi contact materials to arc erosion.

This study provides a theoretical basis for screening doping elements to improve the performance of AgNi electrical contact materials and offers new ideas in this field.

**Author Contributions:** Conceptualization, J.W.; Methodology, J.W. and Y.Z.; Software, J.W.; Validation, Y.Z.; Investigation, Y.Z. and M.W.; Resources, J.C. and G.H.; Writing—original draft, Y.Z. and M.W.; Writing—review & editing, Y.Z., J.C. and G.H.; Visualization, Y.Z.; Supervision, J.W. All authors have read and agreed to the published version of the manuscript.

**Funding:** This research was funded by [S&T Program of Hebei] grant number [225676163GH].

**Institutional Review Board Statement:** Not applicable.

**Informed Consent Statement:** Not applicable.

**Data Availability Statement:** Data are contained within the article.

**Conflicts of Interest:** Author Jing Chen and Guanglin Huang were employed by the company Wenzhou Juxing Electric Contact Technology Co., Ltd. The remaining authors declare that the research was conducted in the absence of any commercial or financial relationships that could be construed as a potential conflict of interest.

## References

- Guzmán, D.; González, F.; Muranda, D.; Aguilar, C.; Guzmán, A.; Soliz, Á.; Lozada, L.; Iturriza, I.; Castro, F. Fabrication and Arc Erosion Behavior of Ag-SnO<sub>2</sub>-ZnO Electrical Contact Materials. *Materials* **2023**, *16*, 3618. [[CrossRef](#)] [[PubMed](#)]
- Jug, A.; Brunčko, M.; Rudolf, R.; Anžel, I. Oxidation Behaviour of Microstructurally Highly Metastable Ag-La Alloy. *Materials* **2022**, *15*, 2295. [[CrossRef](#)]
- Swingler, J. Performance and arcing characteristics of Ag/Ni contact materials under DC resistive load conditions. *IET Sci. Meas. Technol.* **2011**, *5*, 37–45. [[CrossRef](#)]
- Wu, C.P.; Yi, D.Q.; Li, J.; Xiao, L.R.; Wang, B.; Zheng, F. Investigation on microstructure and performance of Ag/ZnO contact material. *J. Alloys Compd.* **2008**, *457*, 565–570. [[CrossRef](#)]
- Li, G.; Yang, T.; Ma, Y.; Feng, W.; Zhang, X.; Fang, X. Mechanical characteristics of the Ag/SnO<sub>2</sub> electrical contact materials with Cu<sub>2</sub>O and CuO additives. *J. Alloys Compd.* **2020**, *817*, 152710. [[CrossRef](#)]
- Yangfang, C.; Xiaofang, Y.; Xiaoping, B.; Mingjiang, Z.; Jie, L.; Changlin, Y.; Xiufang, Z. Research on the Influence of Different Oxide Particles on Properties of AgCdO Contact Material. *J. Phys. Conf. Ser.* **2021**, *1948*, 012192. [[CrossRef](#)]
- Zheng, J.; Jiang, F.; Li, S.L. Study on New Types of Environmental Protection AgSnO<sub>2</sub> Electrical Contact Materials. *Adv. Mater. Res.* **2013**, *815*, 400–403. [[CrossRef](#)]
- Xiaolong, Z.; Qiyang, T.; Yunhong, Z. Microstructure and Properties of AgSnO<sub>2</sub> Composites by Accumulative Roll-bonding Process. *Rare Met. Mater. Eng.* **2017**, *46*, 942–945. [[CrossRef](#)]
- Kim, S.K. Process development of low-cost AgNi and AgFe contact materials with no range of solid solubility. *Adv. Mater. Res.* **2008**, *47*, 873–876. [[CrossRef](#)]
- Wang, H.; Yuan, H. Investigation on the electrical properties of AgNi contact materials with various Ni content. In Proceedings of the 2017 IEEE Holm Conference on Electrical Contacts, Denver, CO, USA, 10–13 September 2017; pp. 221–224.
- Cenci, M.P.; Scarazzato, T.; Munchen, D.D.; Dartora, P.C.; Veit, H.M.; Bernardes, A.M.; Dias, P.R. Eco-friendly electronics—A comprehensive review. *Adv. Mater. Technol.* **2022**, *7*, 2001263. [[CrossRef](#)]
- Cho, H.; Hwang, D.Y.; Jo, H.H. A study on the development of environment-friendly Ag-SnO<sub>2</sub> electric contact materials through a powder metallurgy. *Mater. Sci. Forum* **2007**, *539*, 2761–2766. [[CrossRef](#)]
- Li, H.; Wang, X.; Liang, Y.; Hu, Z.; Guo, X. Fabrication and characterization of Ag-4wt.%TiB<sub>2</sub>-4wt.%Ni contact materials utilizing coarse and ultrafine Ag powders. *Vacuum* **2020**, *182*, 109756. [[CrossRef](#)]
- Wang, X.; Yang, H.; Chen, M.; Zou, J.; Liang, S. Fabrication and arc erosion behaviors of AgTiB<sub>2</sub> contact materials. *Powder Technol.* **2014**, *256*, 20–24. [[CrossRef](#)]
- Ivanović, A.; Milojević, S.; Marjanović, V.; Madić, B. Production The High Electric Conductive Materials for Contacts Based on Silver by the Use of Sintermetallurgical Method. In Proceedings of the 15th International Research/Expert Conference “Trends in the Development of Machinery and Associated Technology”, TMT, Prague, Czech Republic, 12–18 September 2011; pp. 12–18.
- Wang, J.; Wang, M.; Zhang, Y. Simulation calculation and experimental study on the properties of Re, In, and Nb-doped Ag/Ni electrical contact materials. *IEEE Trans. Compon. Packag. Manuf. Technol.* **2024**, *14*, 619–629. [[CrossRef](#)]

17. Lin, Z.; Liang, Y.; Zeng, Y.; Chen, X.; Liu, M.; Dai, P.; Chen, J.; Sun, X. Morphology-tunable synthesis and formation mechanism of SnO<sub>2</sub> particles and their application in Ag–SnO<sub>2</sub> electrical contact materials. *Ceram. Int.* **2022**, *48*, 6052–6061. [[CrossRef](#)]
18. Haitao, W.; Mei, Z.; Menglin, Y.; Jingqin, W.; Yancai, Z. Properties of doped Ag–SnO<sub>2</sub> electrical contact materials with different SnO<sub>2</sub> particle sizes. *Mater. Res. Express* **2019**, *6*, 016558. [[CrossRef](#)]
19. Shen, Y.; Qiao, Y.; Jin, T.; Yu, S.; He, Z. AgNi alloy nanoparticles embedded SiO<sub>2</sub> films: Synthesis and structure. *Mater. Lett.* **2015**, *152*, 1–4. [[CrossRef](#)]
20. Hlungwani, D.; Ledwaba, R.S.; Ngoepe, P.E. First-Principles Study on the Effect of Lithiation in Spinel Li<sub>x</sub>Mn<sub>2</sub>O<sub>4</sub> (0 ≤ x ≤ 1) Structure: Calibration of CASTEP and ONETEP Simulation Codes. *Materials* **2022**, *15*, 5678. [[CrossRef](#)]
21. Carmona-Espindola, J.; Gázquez, J.L.; Vela, A.; Trickey, S.B. Generalized gradient approximation exchange energy functional with correct asymptotic behavior of the corresponding potential. *J. Chem. Phys.* **2015**, *142*, 054105. [[CrossRef](#)]
22. Tang, Q.; Hu, G.; Fung, V.; Jiang, D.-E. Insights into interfaces, stability, electronic properties, and catalytic activities of atomically precise metal nanoclusters from first principles. *Acc. Chem. Res.* **2018**, *51*, 2793–2802. [[CrossRef](#)]
23. Schneider, M.; Unger, R.S.; Mitdank, R.; Müller, R.; Krapf, A.; Rogaschewski, S.; Dwelk, H.; Janowitz, C.; Manzke, R. Evolution of the density of states at the Fermi level of Bi<sub>2–y</sub>Pb<sub>y</sub>Sr<sub>2–x</sub>La<sub>x</sub>CuO<sub>6+δ</sub> and Bi<sub>2</sub>Sr<sub>2–x</sub>La<sub>x</sub>CuO<sub>6+δ</sub> cuprates with hole doping. *Phys. Rev. B* **2005**, *72*, 014504. [[CrossRef](#)]
24. Carbó-Dorca, R.; Bultinck, P. Quantum Mechanical Basis for Mulliken Population Analysis. *J. Math. Chem.* **2004**, *36*, 231–239. [[CrossRef](#)]
25. Zhang, X.; Zhang, Y.; Tian, B.; An, J.; Zhao, Z.; Volinsky, A.A.; Liu, Y.; Song, K. Arc erosion behavior of the Al<sub>2</sub>O<sub>3</sub>-Cu/(W, Cr) electrical contacts. *Part B Eng.* **2019**, *160*, 110–118. [[CrossRef](#)]
26. Wu, C.; Zhao, Q.; Li, N.; Wang, H.; Yi, D.; Weng, W. Influence of fabrication technology on arc erosion of Ag/10SnO<sub>2</sub> electrical contact materials. *J. Alloys Compd.* **2018**, *766*, 161–177. [[CrossRef](#)]
27. Swingler, J.; Sumption, A. Arc erosion of AgSnO<sub>2</sub> electrical contacts at different stages of a break operation. *Rare Met.* **2010**, *29*, 248–254. [[CrossRef](#)]
28. Berger, H.H. Contact resistance and contact resistivity. *J. Electrochem. Soc.* **1972**, *119*, 507. [[CrossRef](#)]
29. Zhang, L.; Liu, Y.; Song, H.; Wang, S.; Zhou, Y.; Hu, S.J. Estimation of contact resistance in proton exchange membrane fuel cells. *J. Power Sources* **2006**, *162*, 1165–1171. [[CrossRef](#)]
30. Liang, P.; Qiu, D.; Peng, L.; Yi, P.; Lai, X.; Ni, J. Contact resistance prediction of proton exchange membrane fuel cell considering fabrication characteristics of metallic bipolar plates. *Energy Convers. Manag.* **2018**, *169*, 334–344. [[CrossRef](#)]
31. Sedlaček, M.; Podgornik, B.; Vižintin, J. Influence of surface preparation on roughness parameters, friction and wear. *Wear* **2009**, *266*, 482–487. [[CrossRef](#)]
32. Jurevicius, M.; Skeivalas, J.; Urbanavicius, R. Analysis of surface roughness parameters digital image identification. *Measurement* **2014**, *56*, 81–87. [[CrossRef](#)]
33. Gold, G.; Helmreich, K. A physical surface roughness model and its applications. *IEEE Trans. Microw. Theory Tech.* **2017**, *65*, 3720–3732. [[CrossRef](#)]

**Disclaimer/Publisher’s Note:** The statements, opinions and data contained in all publications are solely those of the individual author(s) and contributor(s) and not of MDPI and/or the editor(s). MDPI and/or the editor(s) disclaim responsibility for any injury to people or property resulting from any ideas, methods, instructions or products referred to in the content.